Available online at www.sciencedirect.com
ScienceDirect
International Journal of Multiphase Flow 33 (2007) 432–447
International Journal of Multiphase Flow
www.elsevier.com/locate/ijmulflow

Measurements of rivulet flow between parallel vertical plates

Glenn E. McCreery *, Paul Meakin, Donald M. McEligot [1]

Idaho National Laboratory, Idaho Falls, ID 83415-3885, USA

Received 7 June 2006; received in revised form 27 September 2006

Abstract

The research presented considers laminar, fully-developed rivulet flow in the channel formed by two parallel vertical plates for flows intermediate between a lower limit of droplet flow and an upper limit where the rivulets meander. Although this regime is likely the most simple rivulet flow regime, it does not appear to have been previously investigated in detail. In an earlier paper, the authors derived relations to predict the terminal Reynolds number and non-dimensional width of the rivulet under the approximation that the width is large relative to the gap width of the plates (the spacing between the plates). The objective of the present study is to examine the limits of this simple treatment as the relative width becomes small, i.e., as the rivulets become narrow. Experiments were performed measuring rivulet widths and flow rates for gap widths ranging from 0.152 mm to 0.914 mm with water, light mineral oil, ethyl alcohol and water with a wetting agent. Predictions were found to agree well with the measurements for width-to-spacing ratios as low as unity and less. A numerical analysis shows that a plausible explanation of unexpected agreement for narrow rivulets is that the error in this one-dimensional assumption is approximately countered by the error in neglecting flow in the edge region. To account for curvature of the liquid–air interface at the edges, an additional geometric relationship was assumed; this approach also was found to be a good representation.
Published by Elsevier Ltd.

Keywords: Rivulets; Two-phase flow; Laminar; Fully-developed; Vertical

1. Introduction

Rivulet flow along a single surface (''single-sided'') has been studied extensively during the past four decades. In one of the first studies, Hartley and Murgatroyd (1964) characterized the falling-film-to-rivulet-flow transition using both force and energy criteria. Over time, this work was followed by many other studies that described the film-to-rivulet transition, rivulet geometry, rivulet stability and the transition to meandering flow (Anand and Bejan (1986) defined meandering flow as occurring when bends in the rivulet trajectory of greater than thirty degrees from vertical were observed). A few examples include studies by Towell and Rothfeld (1966), Mikielewicz and Moszynski (1976), Bentwich et al. (1976), Young and Davis (1987), Schmuki

* Corresponding author.
E-mail address: Glenn.McCreery@inl.gov (G.E. McCreery).
[1] Also Professor Emeritus, Aero. Mech. Engr. Dept., U. Arizona and Gastprofessor, IKE, Uni. Stuttgart.

0301-9322/$ - see front matter Published by Elsevier Ltd.
doi:10.1016/j.ijmultiphaseflow.2006.10.003

and Laso (1990), Duffy and Moffat (1995), Alekseenko and colleagues (1995,1996,2005), Hughes and Bott (1998), Johnson et al. (1999), Wilson and Duffy (1998, 2003), Myers et al. (2004), and Le Grand-Piteira et al. (2005). Much of the rivulet flow research has been motivated by the need to characterize heat and mass transfer for high-flux heat exchangers cooled by external flow (i.e., flow over a body or surface rather than internal flow as through ducts) and by geophysical applications. Predictions of the transition from thin film flow to rivulet flow and the rivulet flow geometry provide the flow boundary conditions and heat transfer area for convection to the flowing liquid. An example is the study by McCreery et al. (1989), who studied falling film and rivulet flow distributions and heat transfer for a heated steam generator tube in a vertical orientation.

The work reported in this manuscript was motivated by the need to obtain a better understanding of fluid flow and the transport of contaminants, such as toxic metals and radionuclides, in fractures in the Earth's subsurface. The formation of rivulets allows water and associated contaminants to penetrate further and faster into the subsurface than for film flow. The transition from film flow to rivulet flow is expected to be particularly significant for the penetration of water into partially-saturated, fractured porous materials since reduction in the contact area between the invading fluid and the fracture surfaces will reduce loss of fluid from the fracture aperture (i.e., the space between the walls forming the fracture) by imbibition into the porous matrix. Channeling the flow into rivulets will therefore allow the fluid remaining in the fracture to penetrate further and more rapidly.

In comparison with research on external rivulet flow, rivulet flow confined by two surfaces (''double-sided'') has received almost no attention despite applications such as flow in geological fractures and liquid cooling of finned heat exchanger tubes. Anand and Bejan (1986) performed an experimental study of the transition from laminar to turbulent flow for rivulet flow between parallel plates. The transition was marked by an abrupt change to meandering flow, which the authors described as being a similar phenomenon to buckling of fluid layers. Su et al. (2001) studied solute transport in unsaturated fractures both experimentally and analytically. Their investigations included intermittent rivulet flow, which the authors characterized as ''snapping rivulet'' and ''pulsating blob'' modes. Nicholl et al. (1994) reported research on the gravity-driven wetting front instability in initially dry fractures with experiments that employed a transparent simulated fracture with rough walls. Fernandez et al. (2001) investigated wavelength selection of fingering instabilities in Hele–Shaw cells. Drenckhan et al. (2004) investigated wave formation on rivulets of surfactant solution flowing between narrowly spaced glass plates and formulated relationships between wavelength, amplitude, and plate separation. The relationships lead to a prediction of the stable to meandering rivulet flow transition. Stedtfeld et al. (2005) investigated multiphase flow in parallel-wall channels and simulated fracture apertures. The effect of Bond number, the ratio of gravity to capillary forces, was varied by employing a centrifuge to vary the body force representing gravity. Flow regimes, including rivulet flow, and regime transitions were characterized.

Gravity-driven instabilities occur when a dense fluid overlies a lighter fluid and the combination of capillary and viscous forces is not sufficient to stabilize the displacement front. The resulting liquid fingers penetrate the fracture. The initial finger width for displacement of gas by liquid may be predicted for flow in narrow parallel-wall channels (a.k.a. Hele–Shaw cells) using linear stability theory. A rivulet may be formed when a finger that has propagated through the channel continues to be supplied with liquid. The width of the finger is typically considerably wider than that of the ensuing rivulet because capillary force at the advancing finger tip retards its penetration into the aperture. When fluid is injected at one position at the top of an initially dry parallel channel, the initial flow consists of a large slow-moving drop with a trailing rivulet attached, as shown in Fig. 1. If the flow rate is sufficiently large, the rivulet is maintained after the drop has drained. If the flow is below a critical lower limit, the rivulet breaks and a new drop with a trailing rivulet will form (Stedtfeld et al., 2005). The new drop and subsequent drops are smaller and faster moving than the initial drop because wetting is facilitated by a thin layer of fluid deposited on the walls by the initial drop. As the flow rate is further increased, the rivulets begin to meander with approximately sinusoidal paths. At even higher flow rates, the meandering is unstable and the trajectory whips about as an out-of-control garden hose does. The rivulet may then break into a number of separate rivulets which may again combine and break in a chaotic fashion.

McCreery and McEligot (2004) applied the assumptions and approximations of Anand and Bejan (1986) to the simpler situation of a fully-developed rivulet flow. In this case, the dominant phenomena reduce to the viscous stresses and gravity so that dimensional reasoning shows that the rivulet width should be proportional to the quantity $Q\nu/g\delta^3$ – where Q is the volumetric flow rate, ν is the kinematic viscosity, g is the acceleration

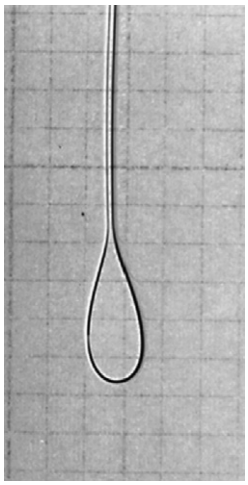

Fig. 1. Photograph of water drop with trailing rivulet.

of gravity and δ is the plate spacing (Peregrine, 2004). (However, the dimensional analysis does not provide the constant of proportionality). It is predicted that the terminal velocity, the final velocity achieved when viscous force balances gravitational force, and Reynolds number (based on twice the plate spacing) depend on the spacing and fluid properties and are independent of the total flow rate; the rivulet spreads to accommodate the imposed flow. The analysis was based on the assumption that the width in the spanwise direction is considerably larger than the spacing, so edge effects could be neglected. Since the edge region includes additional wall shear stress and an addition to the gravitational body force, the errors involved in neglecting this region may counter each other to some extent. Thus, one may expect that the predictions would apply to narrower rivulets than implied by the assumption. While a two-dimensional numerical solution has been conducted, it is also appropriate first to examine the need experimentally. Accordingly, the main objective of the present work is taken to be to determine the limits of the simple treatment as the rivulet width becomes small in comparison with gap width. Emphasis is on laminar flows between the lower flow drop regime limit and the upper meandering flow limit. The experimental method, experiment uncertainties and data are described; predictions using the simple approach and related extensions are compared with experimental results.

2. Analytical considerations

For "narrow" rivulets the horizontal cross-section can described as shown in Fig. 2 where an inner width W_i and an outer width W_o are defined. The geometry of the liquid–gas interface is approximately circular since the imposed gas pressure and the internal liquid pressure are constant and the constant differential pressure, calculated from the Laplace equation (de Gennes et al., 2004), is equal to σ/r where σ is the surface tension and r is the radius (this representation is based on the assumption that the radius in the flow direction is infinite). If

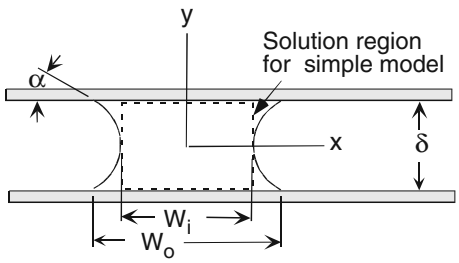

Fig. 2. Schematic diagram of rivulet cross-section with nomenclature employed. The solution region for the simple solution is shown.

one approximates the liquid–air interface as a circular arc, the trigonometric relationship between these two widths is (McCreery et al., 2005)

$$(W_o - W_i)/\delta = (1 - \sin\alpha)/\cos\alpha$$

where α is the contact angle (Fig. 2). That is, the non-dimensional extent of the edge region is predicted to be a function of contact angle alone. The width difference ($W_o - W_i$) then increases directly as the spacing does.

For completeness, we repeat the assumptions and approximations of McCreery and McEligot (2004). For this treatment, we orient the coordinates such that z is vertical, x is spanwise, and y is normal to the vertical plates, as shown in Fig. 2, and assume

- the fluid is incompressible and has constant properties,
- flow is steady and laminar,
- fluid density is constant and much greater than density of its surroundings,
- interface shear with surroundings is negligible at the edges ($\partial V_z/\partial x \approx 0$),
- flow is fully-developed away from the inlet,
- the inner width W_i is much greater than the distance between it and the outer width W_o, hence the curved interface region can be neglected.

Under these assumptions and approximations, it can be shown from a force balance between gravity and viscous forces that the flux

$$Q = \delta V_b W = \frac{gW\delta^3}{12\nu}$$

where, V_b is the bulk or average velocity and W corresponds to W_i in Fig. 2.

Stated in non-dimensional terms,

$$\frac{Wg\delta^3}{Q\nu} = 12$$

The Reynolds number is then,

$$Re = \frac{V_b 2\delta}{\nu} = \frac{2Q}{\nu W} = \frac{g\delta^3}{6\nu^2}$$

The Reynolds number depends on the plate spacing and fluid properties and is independent of the total flow rate. Thus, for a given spacing, increasing the imposed flow rate leads to spreading the rivulet width but does not affect the Reynolds number. The choice of 2δ as the characteristic dimension is retained to be consistent with the development by McCreery and McEligot (2004); it is the hydraulic diameter of the idealized flow region, not including the hypothesized non-flow edge region.

3. Experimental method

As noted above, the main objective of the present study is to examine the limits of this simple treatment as the relative width W_i/δ becomes small, i.e., as the rivulets become narrow. Accordingly, experiments were conducted to characterize rivulet flow between two vertically-oriented parallel glass plates with dimensions 30.5 cm by 14 cm using the apparatus shown in Fig. 3. The gap width was set by clamping spacers (shims) between the two glass plates as shown in Fig. 3b. Average gap widths used in these experiments were 0.168 mm, 0.419 mm, 0.597 mm and 0.902 mm. The variation of these values was approximately $\pm$0.012 mm; this variation was determined by use of feeler gages, which have thickness tolerances of approximately $\pm$0.005 mm. Rivulet inner and outer widths (W_i and W_o in Fig. 2) were measured as functions of flow rate for several fluids: water, water plus wetting agent (Kodak PhotoFlo solution mixed 8 parts per 10,000 water), ethyl alcohol and light mineral oil. Relevant fluid properties are listed in Table 1 for a temperature of 21 °C; the operating temperature was kept within one degree of this value. The contact angles were measured using the sessile drop method (Schmittbuhl et al., 1993) with a contact angle instrument (Model

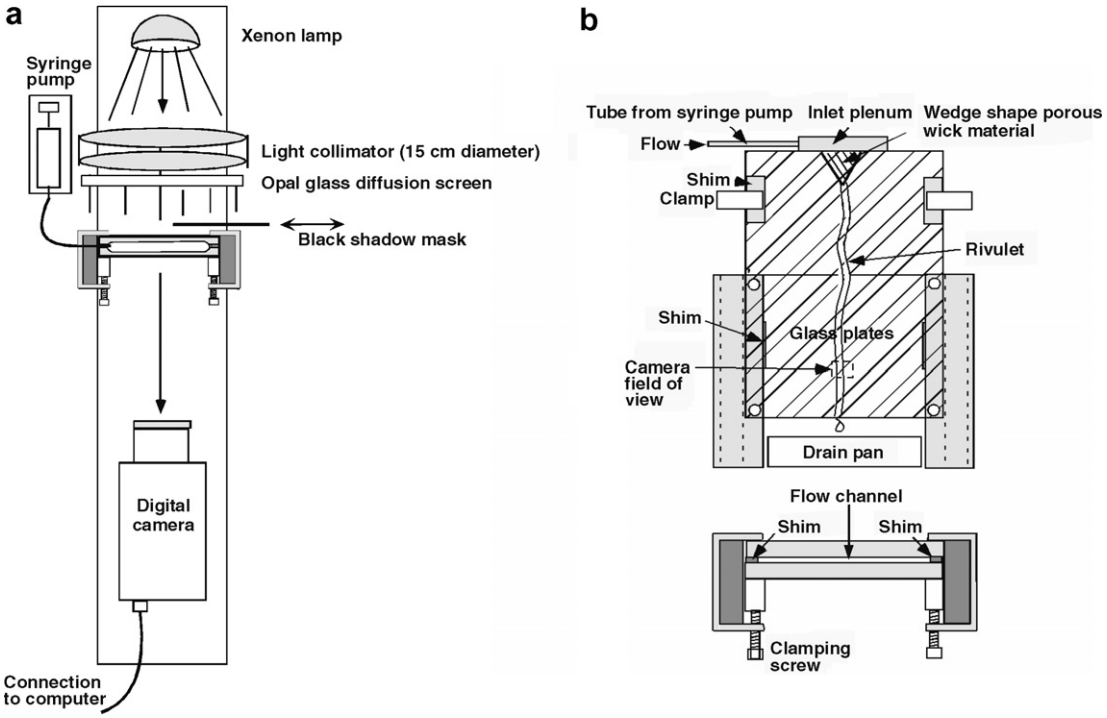

Fig. 3. Schematic diagrams of experiment: (a) top view of overall experiment and (b) top and side views of the flow channel with its holder.

Table 1
Fluid properties[a] and static glass–fluid contact angle[b] at temperature = 21 °C

	Density (kg/m^3)	Kinematic viscosity (m^2/s)	Static contact angle (°)
Water	998	0.98×10^{-6}	15
Water plus Wetting agent (1 part/8000)	998	0.98×10^{-6}	11
Mineral oil	835 ± 2	$1.42 \times 10^{-5} \pm 0.03 \times 10^{-5}$	7
Ethyl alcohol	789	1.18×10^{-6}	5

[a] Fluid properties are from Weast (1971) and, for mineral oil, from Orr et al. (1997).
[b] Contact angle measurements were obtained using an FTA200 Contact Angle Analyzer from First Ten Angstroms, Inc.

FTÅ200 by First Ten Angstroms of Portsmouth, Va.). The results are reported as the average of three contact angle measurements.

Flow was delivered by a KDSyentific model 100 syringe pump with a maximum flow rate of 557 ml/h, a digital readout resolution of 0.1 ml/h and an uncertainty of approximately 1% input flow rate (after calibration). Solitary rivulets were generated at the same initial position by delivering fluid to a wedge-shaped piece of porous material (coffee filter paper) inserted between the two plates. It was necessary to wrap wick material around the inlet tube; otherwise, entrainment of small air bubbles was observed to occur during several unsuccessful experiments. The consequence of air bubbles was to destabilize the flow and cause either oscillations or, in experiments that employed the largest gap width, meandering rivulet flow. The glass plates were cleaned carefully before each experiment using acetone first and then ethyl alcohol.

The rivulets were observed to contract in width below the injection point (due to fluid acceleration by gravity) and then approach an approximately constant width as the terminal velocity was approached. The average width was measured from digital images taken of an area, approximately 20 cm below the entrance, where the rivulets appeared to have reached their terminal velocity. This position provided upstream lengths more than 60 times the spacing. For steady laminar flow between parallel plates, the development length is of the order of $L/\delta \approx 0.02Re$, where L is the distance from entrance (Schade and McEligot, 1971). Therefore, the lower the

Reynolds number *Re* is, the shorter the distance required to approach the fully-developed state. At the maximum Reynolds number of this experiment, this development distance would be about 30 times the spacing. The distance from the measurement position to the channel exit (approximately 10 cm) was sufficient to insure that exit effects did not disturb flow in the measurement region.

The measurement area imaged by the camera was typically 19.60 mm by 14.90 mm. For experiments that employed the minimum gap width, porous sponge material was placed at the channel exit to wick away liquid and to prevent the formation of a liquid column above the exit due to capillary forces. Experiments that employed larger gap widths drained freely and wicking at the channel exit was not necessary.

The boundaries of the inner part of the rivulet are prominently visible as dark lines in images due to the effects of refraction and total internal reflection at the fluid–air interfaces as shown in Figs. 4 and 5. The outer rivulet boundary was not visible unless an additional technique of interposing a black mask between the diffuse light source and rivulet boundary was used as also shown in Figs. 4 and 5. The mask was manually placed

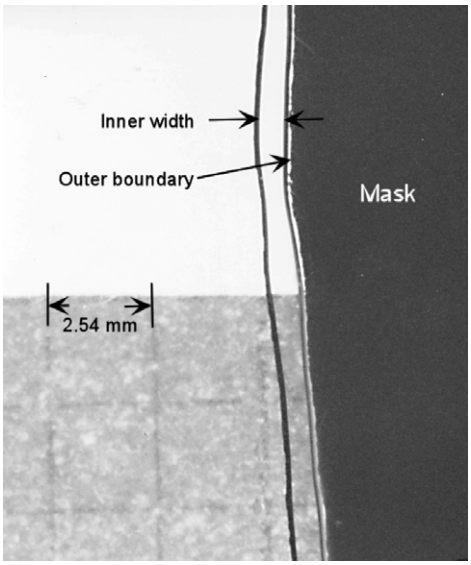

Fig. 4. Photograph of typical rivulet demonstrating masking process.

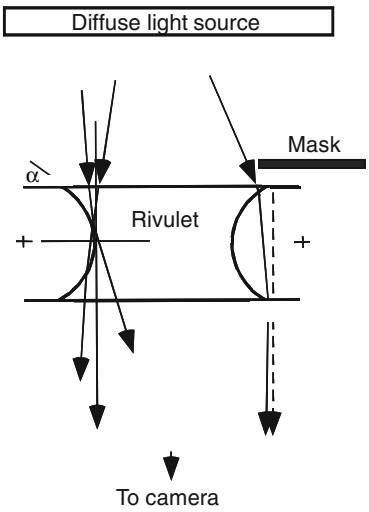

Fig. 5. Examples of light paths through a rivulet.

in a position so that white light was refracted to the camera from inside the rivulet boundary, thereby contrasting with the black mask immediately outside the rivulet boundary. Although dye mixed in the fluid made the outer boundary marginally more visible, the dye decreased the contrast of the inner boundary and was not used for the majority of experiments. Use of collimated light rather than diffused light increased the contrast of the inner width boundary but decreased the visibility of the outer boundary. The best compromise was to use diffuse light with the diffuser placed approximately 20 cm behind the channel.

Average rivulet inner width W_i shown in Fig. 2, was measured by either of two procedures: (1) For rivulets where the width did not vary significantly with vertical position, the inner pixel width was measured directly at typically five locations and the results were averaged. Average pixel width was then divided by a calibration constant to determine width. (2) For rivulets whose profile varied with position, such as the rivulet shown in Fig. 4, the following method was used:

1. Transform the image to a black and white image via Photoshop Elements 2.0 software (Adobe, 2002).
2. Select the inner boundary using the Photoshop "magic lasso" tool.
3. Color the area within the inner width black.
4. Measure the number of black pixels using ImageJ software (Rasband, 2003).
5. Divide the number of black pixels by the pixel length of the image of the rivulet and employ the calibration constant to provide the average rivulet width in millimeters.

The difference between outer width and inner width ($W_o - W_i$) was determined by measuring the average difference between the outer boundary position and the inner boundary position on the side at which a mask was used to make the outer boundary visible (Figs. 4 and 5). Twice the average difference was then added to the measured inner width to determine the outer width.

The *measured* Reynolds number was calculated from the measured flow rate as

$$Re_{meas} = \frac{V_b 2\delta}{v} = \frac{2Q}{vW_i}$$

in accordance with the assumption that the flow in the edge regions can be neglected.

4. Estimated experimental uncertainties

The experimental results are subject to a number of sources of uncertainty. We believe that the four most important sources of uncertainty are (in order) gap width, the resolution of the rivulet boundaries in the images, parallax in viewing an off-center image of a rivulet and static contact angle. Uncertainties in the resolution of rivulet boundaries and the uncertainty due to parallax result in uncertainties in measured width and Reynolds number. Uncertainties in measured gap width result in uncertainties in predicted values of W_i, W_o and Reynolds number $g\delta^3/6v^2$. The uncertainty of measured contact angle contributes to the uncertainties of the predicted values of ($W_o - W_i$) and hence W_o. The approach of Kline and McClintock (1953) was employed to estimate the propagation of the estimated measuring uncertainties into the results. Some key values are listed in Table 2.

The gap width is set by clamping shims with a tolerance of approximately ±0.005 mm between glass plates. Gap width was measured using feeler gauges with a stated manufacturing tolerance of ±0.005 mm. The variation of measured gap width around the mean was approximately ±0.013 mm. Although this variation is small, it had a large effect on predicted values of rivulet width for the smallest gap width since it enters the prediction to the third power. The uncertainty of predicted W_i, ($12Qv/g\delta^3$), is dominated by the uncertainties in measuring gap width. Based on the manufacturer's stated tolerance for the measurement of contact angle, we estimate that its uncertainty is about is one degree or less. The uncertainty in predicting W_o, using measured gap width, is due to uncertainties in contact angle and in predicted W_i, which is also due to uncertainty in gap width. The uncertainty of *predicted* Reynolds number ($g\delta^3/6u^2$) is dominated by the uncertainty of measured gap width; its percent uncertainty is therefore approximately the same as for the predicted W_i.

The resolution in measuring width from the digital images was approximately three pixels or about ±0.04 mm. The uncertainty of measuring W_o is larger than for W_i since two measurements are added together

Table 2
Estimated experimental uncertainties

Estimated experimental uncertainties				
Gap width δ			±0.013 mm	
Pixel resolution			±0.04 mm	
Parallax			−0.01–0.0 mm	
Measured W_i			±0.04–0.045 mm	
			±7% (high Q)–> 30% (low Q)	
Flow rate Q			±1% of value	
Contact angle α			±1% of angle	
Predicted edge region $(W_o - W_i)/\delta$			Approx. ±1.8% ($5 < \alpha < 15$ deg)	
Measured $Re_m(=2Q/\nu W_i)$			±7% (high Q)–> 30% (low Q)	
Uncertainties related to gap width				
Gap width δ	0.168 mm	0.419 mm	0.597 mm	0.902 mm
Measured gap width δ	±7.7%	±3.1%	±2.2%	±1.4%
Predicted $W_i(=12Q\nu/g\delta^3)$	±23%	±9.4%	±6.6%	±4.4%
Predicted $(W_o - W_i)$	±7.9%	±3.6%	±2.8%	±2.3%
Predicted $Re(=g\delta^3/6\nu^2)$	±23%	±9.3%	±6.5%	±4.3%

to determine this width; this contribution to the uncertainty in W_o is approximately ±0.06 mm. An additional uncertainty in measuring W_i was due to the parallax between the near and far walls of the channel for an off-center rivulet. Parallax was minimized by placing the camera lens approximately 40 cm from the flow cell and using the maximum focal length available on the zoom lens. The angular field of view was thereby reduced to approximately 3°. The concave fluid surfaces bounding W_i also contribute to minimizing parallax error. The maximum uncertainty due to parallax was calculated to be approximately −0.01 mm (parallax error always reduces the measured width) for the largest gap widths; it is proportional to gap width and therefore smaller for experiments with smaller gap widths.

The maximum estimated uncertainty in W_i data is a combination of the pixel resolution and the parallax uncertainties. It varied from approximately ±0.04 mm for the smallest gap width to approximately ±0.045 mm for the largest. The relative uncertainty of measured W_i varied from approximately 7% of measurement at the highest flow rates to 30% at the lowest. Exceptions are for the experiments that used water or water plus wetting agent for flow through the largest gap width. For those experiments the relative uncertainty varied from approximately 15% at the highest flow rates to ±65% at the lowest. The uncertainty in *measured* Reynolds number $(=2Q/\nu W_i)$ is dominated by the uncertainty of measured W_i. The percent uncertainty of Re_m is therefore approximately equal to that of W_i.

5. Experimental results and discussion

Measurements with the four fluids were obtained over a range of gap widths giving $\sim 5 < Re_{meas} < 1400$. With these fluids and gap widths, imposed flow rates were varied to yield non-dimensional inner widths over a range $\sim 0.05 < W_i/\delta < \sim 90$. Tabulations of the data and additional presentations of results are provided in a technical report by McCreery et al. (2005).

Figs. 6 and 7 provide typical examples of the data in terms of the quantities measured directly. gap widths δ (denoted "gap widths") are indicated on the ordinates for comparisons to allow visual estimates of the aspect ratio W_i/δ. Also shown are the predictions from the simple analysis of McCreery and McEligot (labeled "calculated") for the same conditions. Predictions of W_i use measured values of flow rate and gap width; they are presented as two lines in each graph, one representing the gap width at minimum tolerance and one at maximum tolerance. In Fig. 6 predictions for the average measured gap width ($\delta = 0.168$ mm) are shown as a third curve which agrees well with the data. Predictions of W_i agreed well with measured values and were within the estimated experimental uncertainties. In accordance with the simple analysis, an approximately linear relationship between W_i and flow rate was maintained for W_i considerably smaller than gap width for all experiments, except for the one experiment which employed the minimum gap width of 0.168 mm.

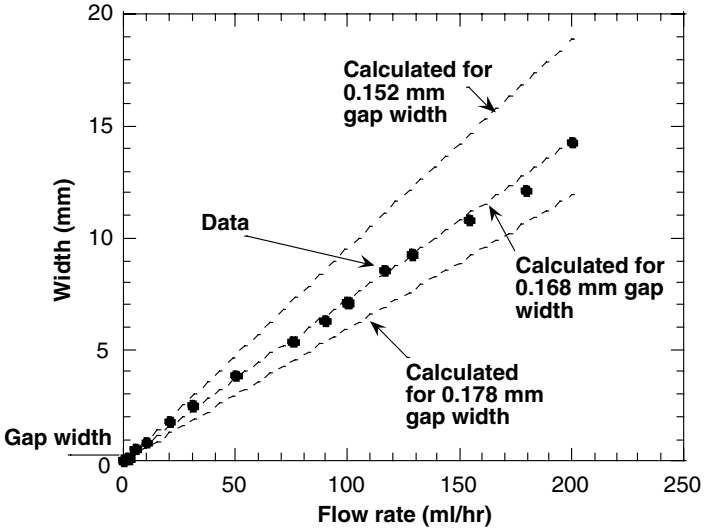

Fig. 6. Width comparisons for measurements and predictions based on simple approach (McCreery and McEligot, 2004) for water flow between vertical plates spaced at 0.168 mm average gap width. Predictions are also given for gap widths at minimum and maximum tolerances (W_o is not distinguishable from W_i in this experiment).

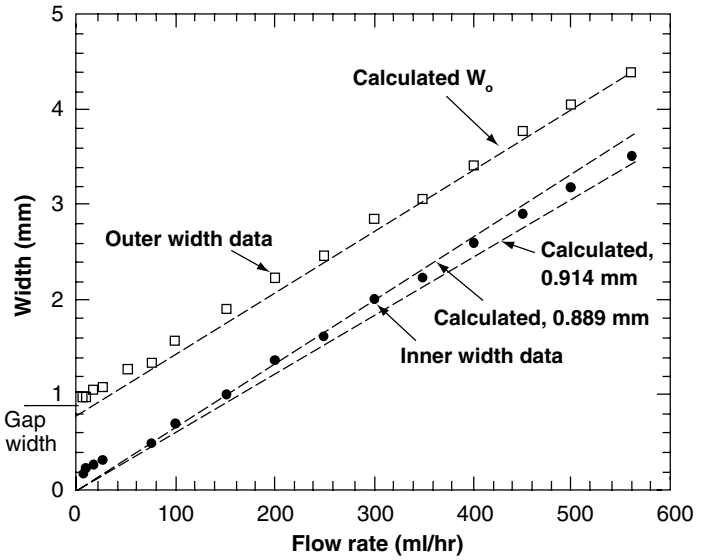

Fig. 7. Width comparisons for measurements and predictions based on simple approach for flow of mineral oil between vertical plates spaced at 0.902 mm.

Fig. 6 shows behavior with water for small gap widths at flow rates leading to wide rivulets. Resulting widths reach fourteen times the gap width. This situation is the basis for the assumptions mentioned earlier; due to the small gap width, the extent of the edge region ($W_o - W_i$) is negligible relative to the rivulet width. Since the assumptions are essentially met, the agreement between prediction and data is excellent, as one would expect. However, even at low flow rates – where the width becomes comparable to the gap width – the agreement appears good.

In Fig. 7 with mineral oil as the fluid, at low flow rates there are measurements where inner widths are less than the gap width. At flow rates lower than about 150 ml/h, the neglected edge region is larger than the central region which is treated alone in the simple analysis. Yet the prediction continues to follow the data. And

for this "large" gap width the circular arc approximation leads to reasonable estimates of the size of the edge region and therefore W_o. Based on such observations, we took the main objective of this study to be to determine the limits of the simple analysis as the relative width becomes small.

Predicted values of *outer rivulet width* (W_o) agree with experimental results to within about 20% or better. Predicted values of W_o were based on the averages of the gap width measurements and the inner width. As indicated earlier, some uncertainty in measuring the outer width is attributed to the difficulty of measuring it in comparison with the inner width. An uncertainty of the contact angle of the order of one degree will result in an uncertainty of predicted ($W_o - W_i$) of approximately 3% of gap width for the range of angles measured. Contact line dynamics may also contribute to this uncertainty since an effective contact angle is known to vary considerably due to motion of a contact line. Advancing contact lines usually have contact angles that are larger than the static contact angle and receding contact lines typically have contact angles that are smaller than the static contact angle (Hewitt et al., 1982). However, the experiments of Rio et al. (2004) showed the contact angle around a dry patch is nearly constant and equal to the static advancing angle, at least when the evolution of its shape is followed for increasing flow rates. Although the assumption of a static rivulet boundary is accurate for most present cases, the rivulet boundaries were observed to move slowly in other cases.

The prediction that the non-dimensional width $gW_i\delta^3/Q\nu$ is approximately equal to twelve is examined in Fig. 8 as a function of W_i/δ. In the figure it has been normalized via division by twelve so agreement is represented by a value of unity. As emphasized earlier in the assumptions of the simple treatment, agreement is expected for W_i/δ significantly greater than unity and, in general, it is seen. With the exception of the run for water with the narrowest gap width = 0.168 mm (circles), most data confirm the prediction down to W_i/δ less than unity. Some agree to values as low as $W_i/\delta \approx 0.1$, i.e., almost no central region and well beyond the expected validity of the assumption. (The one run which is a bit high at $W_i/\delta > 1$ has the smallest gap width so its percent sensitivity to measurement of δ^3 is greatest, about 23% which is the order of the difference seen.)

The consequence that the Reynolds number is independent of flow rate is examined with Fig. 9. The measured Reynolds number, $Re_{meas} = 2Q/\nu W_i$, is normalized by the predicted value, $Re_{pred} = g\delta^3/6\nu^2$, which is still sensitive to the measured gap width. Since flow rate is predicted to be proportional to rivulet width for a given fluid and gap width, the abscissa is again chosen to be W_i/δ. Low flow rates are therefore on the left and high ones on the right. One sees that the normalized Reynolds number is approximately independent of flow rate until W_i/δ is reduced to about unity or less where the width prediction weakens. Since the ratio of measured to predicted Reynolds numbers, Re_{meas}/Re_{pred}, is the reciprocal of the normalized width shown in Figs. 8 and 9 is essentially the inverse of Fig. 8 and one sees a one-to-one correspondence between the

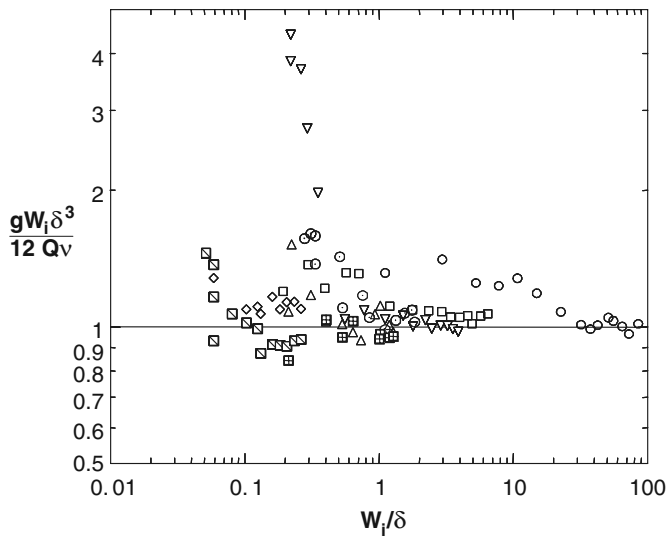

Fig. 8. Non-dimensional width measurements normalized by prediction of simple approach. (Water: circles, $\delta = 0.168$ mm; squares, $\delta = 0.419$ mm; triangles, $\delta = 0.597$ mm; diamonds, $\delta = 0.902$ mm; water with wetting agent: crossed square, $\delta = 0.597$ mm; diagonal-square, $\delta = 0.902$ mm; mineral oil: inverted triangle, $\delta = 0.902$ mm; ethanol: dotted circles, $\delta = 0.597$ mm.)

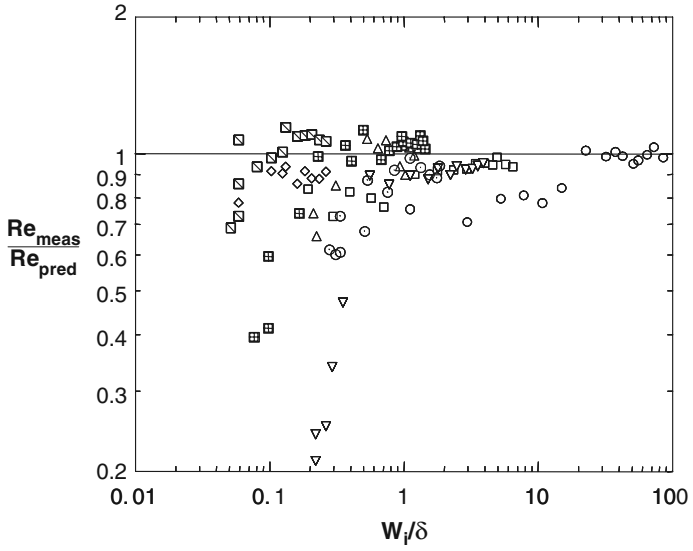

Fig. 9. Comparisons between measured Reynolds numbers and those predicted via simple approach (symbols as in Fig. 8).

individual data points, low Reynolds number for high width and vice versa. Again the data for water with $\delta = 0.168$ mm (circles) show the greatest disagreement for $1 < W_i/\delta < \sim 12$ and the trend of the Reynolds number data for mineral oil at $W_i/\delta < \sim 0.4$ mirrors its width data (inverted triangles).

While more exact analysis is beyond the scope of the present work, one can use a *numerical treatment* to reveal one explanation for the unexpected agreement. The finite-element code FlexPDE (PDE Solutions, 2004) was applied to steady laminar flow between two parallel plates. FlexPDE is a general, partial-differential-equation solver that uses the finite element method for numerical solutions of boundary value problems. The present solution was applied to a three-dimensional region. The geometry was confined to a half rivulet with a given contact angle and a semi-circular liquid–air interface. The body force per unit volume was set equal to ρg. No-slip conditions were prescribed on the plates and no-shear (free slip) conditions were imposed along the cylindrical interface between liquid and gas. An example of the predicted velocity distributions is shown in Fig. 10 for an aspect ratio of $W_i/\delta = 1.633$ and a typical water-glass contact angle of fifteen degrees. This plot is a two-dimensional slice through the calculation domain. The contours of the velocity component in the rivulet flow direction (vertical) are normalized by their maximum value which occurs at the 0, 0 coordinate. In the edge region one sees flow (i.e., not zero velocity) that was not treated in the simple analysis of McCreery and McEligot (2004). On the other hand, in the central region the distribution is not one-dimensional in the spanwise direction as assumed in the analysis. Along the centerplane parallel to the plates, the predicted velocity maxima decrease as the free surface is approached. Consequently, the total flow rate in the central region is less than implied by the assumptions of the simple analysis. These two effects – additional flow in the edge region and reduced flow in the center – apparently counter each other so that the predicted width and Reynolds numbers show reasonable agreement with measurements even for narrow rivulets (i.e., $W_i < \delta$).

Calculations with the finite element code were conducted with a typical contact angle of fifteen degrees for water over a range of rivulet and gap widths. A comparison of the numerically predicted flow rate Q_{FE} and the simple approximation Q_{simple} is presented in Fig. 11 for this wetting angle. The ratio of flow rates *for a given aspect ratio* is

$$Q_{FE}/Q_{simple} = \frac{\int V_z \, dA}{\left(\frac{g\delta^3 W_i}{12\nu}\right)}$$

where A is the flow area normal to the flow direction and V_z is the velocity component in the flow direction. The flow rate ratio is solely a function of geometry and not fluid properties since one sees, from an

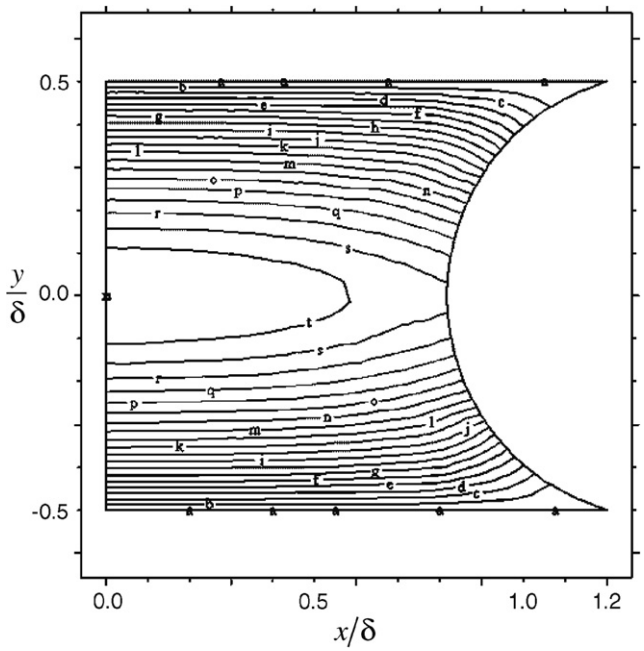

Fig. 10. Example of prediction from three-dimensional finite-element solution showing contours of streamwise (vertical) velocity component (contour interval is 5% of the maximum velocity, which occurs at the coordinates 0, 0).

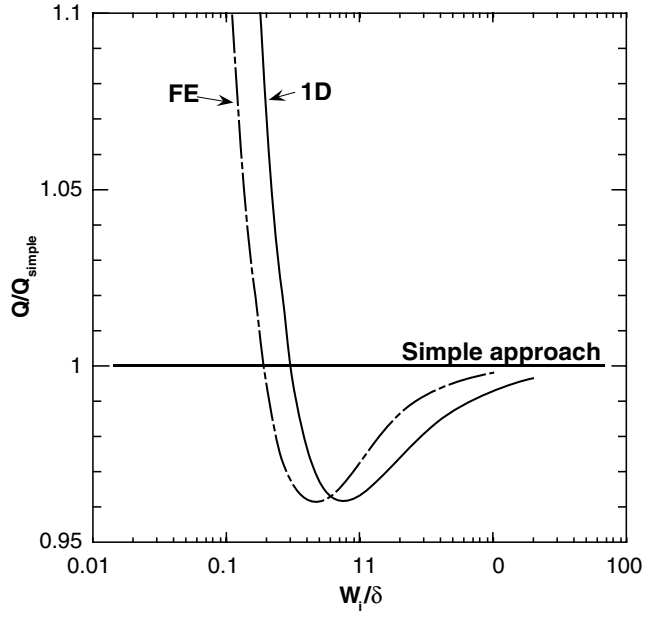

Fig. 11. Flow rate predictions of finite-element approach (centerline marking) and one-dimensional "full-width" treatment (solid line) normalized by prediction from simple approach (unity).

examination of the Navier–Stokes formulation for this problem, that V_z is proportional to ρg and inversely proportional to μ.

In addition to the finite element predictions, a second *one-dimensional approximation* was derived for comparisons (McCreery et al., 2005); in this case the parabolic laminar velocity profile was extended to the

liquid–gas interface and the balance between wall shear and gravity forces included the edge region. The resulting expression for the ratio of flow rates is

$$\frac{Q_{1D}}{Q_{simple}} = \left[W'_i + \frac{1-\sin\alpha}{\cos\alpha} + \frac{1}{2}\tan\alpha - \frac{\pi/2-\alpha}{2\cos\alpha}\right]^2 \frac{\frac{3}{2}V_b}{[W'_i + \frac{1/2(1-\sin\alpha)}{\cos\alpha}]W'_i}$$

where W'_i = aspect ratio = W_i/δ and the average (or bulk) velocity is

$$V_b = Q/A = Q/\left[W_i\delta + \delta^2\left(\frac{1-\sin\alpha}{\cos\alpha} + \frac{1}{2}\tan\alpha - \frac{(\pi/2-\alpha)}{2\cos^2\alpha}\right)\right]$$

Predictions from the finite element and the "full-width," one-dimensional approaches are compared to each other and to the result from the simple treatment in Fig. 11 in terms of the non-dimensional flow rate $12\nu Q/gW_i\delta^3$. One sees that the three curves approach close agreement for aspect ratios of ten or so, as expected. However, the agreement is still within about 4% for aspect ratios significantly below unity. For water and W_i/δ greater than about 0.15, the finite element prediction agrees with the simple analysis within 5%. Consequently, despite the expected limitations of its assumptions, we see – from both the two-dimensional numerical treatment and the measurements – that the predictions from the simple analysis appear reasonable down to aspect ratios below unity. (While the non-dimensional flow rate is a function of both contact angle and aspect ratio, finite element predictions for an angle of 5° showed only a slight difference, agreeing with those for 15° within about 1%.)

At first glance, this "full-width" one-dimensional approach might seem superior to the simple approach since the shape of the flow rate versus width curve in Fig. 11 is similar to that of the numerical solution. However, this solution, like the simple approximation, does not satisfy the boundary condition of zero shear stress at the liquid–gas interface (because, although the derivative of velocity with respect to the spanwise direction is zero, the derivative of velocity with respect to distance normal to the interface is not necessarily zero). Also, the one-dimensional treatment does not provide an overall increase in accuracy (note in Fig. 11 that the simple treatment gives closer agreement to the numerical solution for values of W_i/δ greater than about 2 and the one-dimensional treatment gives better agreement for smaller values of W_i/δ, except in a region near 0.2).

Additional limitations on application of the approximate analysis are related to the flow rate, gap width and Reynolds number. When the flow rate is too small, individual droplets are observed rather than the rivulets treated here. If the Reynolds number becomes too high, the rivulets meander.

Most exceptions to the agreement between predictions and measurements occurred at very low flow rates near the drop flow limit where W_i data tended to be larger than predicted for flow rates. Fig. 12 demonstrates this behavior for ethanol flow with a gap width that is of the order of W_i for the range of flow rates employed. Below about 50 ml/h droplets appear instead of steady rivulets. One sees that, as the flow decreases below about 150 ml/h, the W_i data exceed the predicted linear decrease. Fig. 8 showed that in almost all cases the divergence is an increase in measured width of the central region compared to the prediction. A comparison with the finite-element results in Fig. 11 indicates that the simple approximation underpredicts the flow rate for a given width at the smallest aspect ratios (say $W_i/\delta < \sim 0.15$ or so). For most cases with "moderate" to "large" gap widths (0.597–0.902 mm), further decrease in flow area gives droplet flow (an exception is the mineral oil in Fig. 7 maintaining rivulets to the smallest flow rates measurable – while diverging from the prediction). The transition between rivulet and droplet flow displays considerable hysteresis as a function of flow rate change with time. Hysteresis was not investigated in any detail, except to note that rivulet flow may be maintained at lower flow rates for decreasing flow than for increasing. One reason for this result may be that, for decreasing flow rates, the residual lubrication film deposited by successive drops is wider and thicker than for increasing flow rates.

The *meandering flow limit* was investigated by Anand and Bejan (1986), Drenckhan et al. (2004), and Stedtfeld et al. (2005). According to the criterion of Anand and Bejan, meandering flow is likely to be observed when the Reynolds number based on gap width (δ) approaches 2100. The maximum Reynolds number for our experiments was approximately 1400 when based on 2δ. Thus, our maximum Reynolds number would have been about 700 in terms of their definition. Consistent with their (and the other researchers) results,

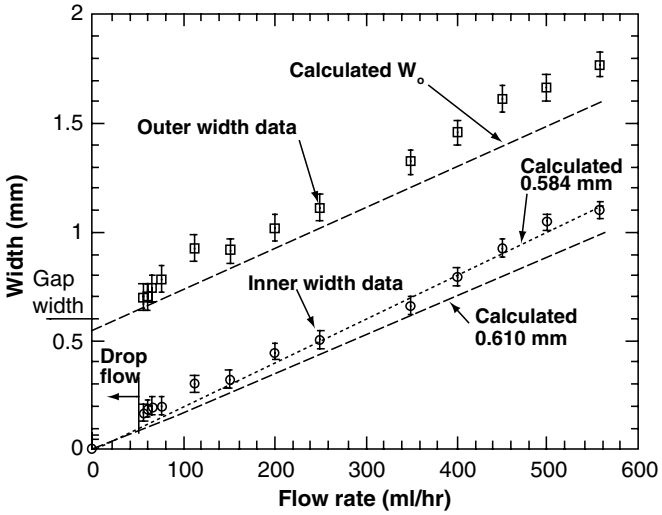

Fig. 12. Width comparisons for measurements and predictions based on simple approach for flow of ethanol between vertical plates spaced at 0.597 mm.

we did not observe meandering flow (which they defined as bends in the rivulet trajectory of greater than thirty degrees from vertical) within the range of the present experiments.

According to Stedtfeld et al. (2005), another flow regime occurs when the gap width is too large to maintain a rivulet attached to both walls. Rivulet flow is then observed attached to one or the other wall or as separate rivulets attached to both walls. However, gap widths were sufficiently small in the present experiments that this regime was not observed and its determination was beyond the scope of the present investigation.

The treatment of McCreery and McEligot – dividing the flow into an inner region, where all the flow occurs, and an outer static region – is a simplification of the actual two-dimensional flow field where streamwise velocity will change continuously from the inner region to the boundaries, as the finite-element results indicate. A full treatment of dynamic laminar (or turbulent) rivulet flow would require a three-dimensional solution of the transient Navier–Stokes equations, with consideration of dynamic contact angles and their hysteresis effects. However, the contact angle may change unpredictably with position due to microscopic surface changes (even for very well cleaned plates); the resulting rivulet width varies slightly with position and the trajectory varies slightly from vertical as Fig. 4 shows. The assumption of steady-state is itself a simplification since rivulets are usually observed to wander at least slightly over time. Slight lateral displacements of a rivulet are restored by capillary forces due to the advancing contact angle being larger than the receding one. Slight wandering is more apparent with fluids having lower viscosity and higher wetting angles. Rivulets of water and ethyl alcohol wander more than those of mineral oil and the addition of a wetting agent to water quiets the wandering despite the lower surface tension. The initial displacements may be due to slight perturbations of fluid injection and formation of small capillary waves. Therefore, we are skeptical that a three-dimensional model would produce a more reliable description of the width and trajectory of a steady rivulet. Although such an approach could provide additional insight into the fluid physics of rivulets, it is well beyond our intent of examining how well a simple technique predicts the general behavior of our data.

6. Concluding remarks

The research presented considers fully-developed, laminar rivulet flow in vertical parallel-wall channels for flows intermediate between a lower limit of droplet flow and an upper limit where the rivulets meander. In a previous paper, the authors derived relations to predict the terminal Reynolds number and non-dimensional width of the rivulet under the approximation that the width is large relative to the gap width of the plates (McCreery and McEligot, 2004). The objective of the present study is to examine the limits of this simple

treatment as the relative width becomes small, i.e., as the rivulets become narrow. Experiments were performed measuring rivulet widths and flow rates for gap widths ranging from 0.152 mm to 0.914 mm with water, light mineral oil, ethyl alcohol and water with a wetting agent.

The various fluids provided a fairly wide range of properties to test the analytical model. The various gap widths and fluids employed provided a range of rivulet Reynolds numbers ranging from approximately 5 to 1400. For any given gap width, the simple treatment and data show that both the rivulet velocity and Reynolds number are approximately constant and that W_i varies approximately linearly with flow rate. Predicted values of inner rivulet width W_i agreed very well with measured values and were mostly within experimental uncertainty for W_i/δ as low as unity and less. Predicted outer rivulet width W_o agreed reasonably well with experimental results within about 20% and less. Results of a finite-element representation of rivulet flow indicate that the agreement at low aspect ratios W_i/δ is due to overprediction of velocity in the central region of the simple approximation compensating, at least partially, for neglecting flow in the edge region. The simple representation of McCreery and McEligot was extended to include the edge region, producing a one-dimensional treatment across the full width. Although the shape of the predicted flow rate versus inner width curve is better predicted by the one-dimensional treatment in comparison to a finite-element analysis, it provides no overall improvement in accuracy compared to the simpler approximation. Consideration of "Occam's razor" (Mainzer, 1994) favors the simpler approach for most applications. It may prove that the one-dimensional model is more accurate for small values of rivulet width compared with gap width. However, the data are not yet sufficient to test this hypothesis. It remains for future studies to extend these initial results to flows in channels with more complex geometry, such as geological fractures.

Acknowledgement

This research was part of a larger program to investigate flow in geological fractures sponsored by the Environmental Management Science Program (EMSP) of the US Department of Energy through DoE Idaho Operations Office contract DE-AC07-05ID14517. We appreciate the kind comments and useful suggestions of the reviewers.

References

Adobe Systems Inc, 2002. Photoshop Elements 2.0. Adobe Systems, Inc., 345 Park Ave., San Jose, Cal. 95110-2704.

Aktershev, S.P., Alekseenko, S.V., 2005. Influence of condensation on the stability of a liquid film moving under the effect of gravity and turbulent vapor flow. Heat Mass Transfer Int. J. 48, 1039–1052.

Alekseenko, S.V., Nakoryakov, V.E., 1995. Instability of a liquid-film moving under the effect of gravity and gas flow. Int. J. Heat Mass Transfer 38, 2127–2134.

Alekseenko, S.V., Markovich, D.M., Shtork, S.I., 1996. Wave flow of rivulets on the outer surface of an inclined cylinder. Phys. Fluids 8, 3288–3299.

Anand, A., Bejan, A., 1986. Transition to meandering rivulet flow in vertical parallel-plate channels. J. Fluids Eng. 108, 269–272.

Bentwich, M., Glasser, D., Kern, J., Williams, D., 1976. Analysis of rectilinear rivulet flow. AIChE J. 22, 772–778.

de Gennes, P.G., Brochard-Wyart, F., Quere, D., 2004. Capillarity and Wetting Phenomena: Drops, Bubbles, Pearls, Waves. Springer, New York.

Drenckhan, W., Gatz, S., Weaire, D., 2004. Wave patterns of a rivulet of surfactant solution in a Hele–Shaw cell. Phys. Fluids 16, 3115–3121.

Duffy, B.R., Moffat, H.K., 1995. Flow of a viscous trickle on a slowly varying incline. Chem. Eng. J. 60, 141–146.

Fernandez, J., Kurowski, P., Limat, L., Petitjeans, P., 2001. Wavelength selection of fingering instability inside Hele–Shaw cells. Phys. Fluids 13, 3120–3125.

Hartley, D.E., Murgatroyd, W., 1964. Criteria for the break-up of thin liquid layers flowing isothermally over solid surfaces. Int. J. Heat Mass Transfer 7, 1003–1015.

Hewitt, G.F., Delhaye, J.M., Zuber, N., 1982. Multiphase Science and Technology, vol. 1. Hemisphere, New York.

Hughes, D.T., Bott, T.R., 1998. Minimum thickness of a liquid film flowing down a vertical tube. Int. J. Heat Mass Transfer 41, 253–260.

Johnson, M.F.G., Schluter, R.A., Miksis, M.J., Bankoff, S.G., 1999. Experimental study of rivulet formation on an inclined plate by fluorescent imaging. J. Fluid Mech. 394, 339–354.

Kline, S.J., McClintock, F.A., 1953. Describing uncertainties in single-sample experiments. Mech. Eng. 75, 3–8.

Le Grand-Piteira, N., Daerr, A., Limat, L., 2005. What governs rivulet meanders on an inclined plane? Cornell university e-prints, http://arxiv.org/PS_cache/physics/pdf/0510/0510089.pdf.

Mainzer, K., 1994. Thinking in Complexity: the Complex Dynamics of Matter, Mind, and Mankind. Springer-Verlag, New York, p. 13.

McCreery, G.E., McEligot, D.M., 2004. Discussion of transition to meandering rivulet flow in vertical parallel-plate channels. J. Fluids Eng. 126, 498–499.
McCreery, G.E., Larson, T.K., Condie, K.G., 1989. Once through steam generator AFW flow distribution and heat transfer. In: Hassan, Y.A. (Ed.), Thermal Hydraulics of Nuclear Steam Generators/Heat Exchangers, vol. 102. ASME HTD, pp. 7–20.
McCreery, G.E., Meakin, P., McEligot, D.M., 2005. Rivulet flow in vertical parallel-wall channels. Tech. report INL/EXT-05-00489, Idaho National Laboratory.
Mikielewicz, J., Moszynski, J.R., 1976. Minimum thickness of a liquid film flowing vertically down a solid surface. Int. J. Heat Mass Transfer 19, 771–776.
Myers, T.G., Liang, H.X., Wetton, B., 2004. The stability and flow of a rivulet driven by interfacial shear and gravity. Int. J. Non-linear Mech. 39, 1239–1249.
Nicholl, M.J., Glass, R.J., Wheatcraft, S.W., 1994. Gravity-driven infiltration instability in initially dry nonhorizontal fractures. Water Resour. Res. 30, 2533–2546.
Orr, B., Thomson, E., Budwig, R., 1997. Drakeol #5 thermophysical property measurements. Tech. report, Mechanical Engineering Dept., Univ. Idaho, 18 December.
PDE Solutions, 2004. Flex PDE Manual, Version 4.2.10. PDE Solutions, Antioch, Cal.
Peregrine, D.H., 2004. Personal communication. School of Mathematics, University of Bristol, 16 March.
Rasband, W., 2003. ImageJ1.29x software. National Institutes of Health, Washington, DC.
Rio, E., Daerr, A., Limat, L., 2004. Probing with a laser sheet the contact angle distribution along a contact line. J. Colloid Interface Sci. 269, 164–170.
Schade, K.W., McEligot, D.M., 1971. Cartesian Graetz problems with air property variation. Int. J. Heat Mass Transfer 14, 653–666.
Schmittbuhl, J., Gentier, S., Roux, S., 1993. Field-measurements of the roughness of fault surfaces. Geophys. Res. Lett. 20, 639–641.
Schmuki, P., Laso, M., 1990. On the stability of rivulet flow. J. Fluid Mech. 215, 125–143.
Stedtfeld, R.D., McCreery, G.E., Stadler, A.T., Stoner, D.H., Meakin, P., 2005. Application of a geocentrifuge and stereolithographically fabricated apertures to investigations of multiphase flow in complex fracture apertures. Int. J. Phys. Modeling Geotech. 5, 27–38.
Su, G.W., Geller, J.T., Preuss, K., Hunt, J.R., 2001. Solute transport along preferential flow pathways in unsaturated fractures. Water Resour. Res. 37, 2481–2491.
Towell, G.D., Rothfeld, L.B., 1966. Hydrodynamics of rivulet flow. AIChE J. 12, 972–980.
Weast, R.C., 1971. CRC Handbook of Chemistry and Physics, 52nd ed. The Chemical and Rubber Company, Cleveland, Ohio.
Wilson, S.K., Duffy, B.R., 1998. On the gravity-driven draining of a rivulet of viscous fluid down a slowly varying substrate with variation transverse to the direction of flow. Phys. Fluids 10, 13–22.
Wilson, S.K., Duffy, B.R., 2003. Strong temperature-dependent-viscosity effect on a rivulet draining down a uniformly heated or cooled slowly varying substrate. Phys. Fluids 15, 827–840.
Young, G.W., Davis, S.H., 1987. Rivulet instabilities. J. Fluid Mech. 176, 1–31.